Applied Geochemistry 152 (2023) 105650



Contents lists available at ScienceDirect

Applied Geochemistry

journal homepage: www.elsevier.com/locate/apgeochem





Americium solubility and solubility limiting solid phase (SLSP) analysis in groundwater of Beishan, a proposed site for the disposal of high-level radioactive waste in China

Sen Yang [a,b], Zeqin Li [a,b], Pujing Pan [a,b,*]

[a] College of Earth Sciences, Chengdu University of Technology, Chengdu, 610059, China
[b] Applied Nuclear Techniques in Geosciences Key Laboratory of Sichuan Province, Chengdu, 610059, China

ARTICLE INFO

Editorial Handling by: Dr Mavrik Zavarin

Keywords:
Americium solubility
High-level radioactive waste (HLW)
Deep geological disposal
PHREEQC
Beishan

ABSTRACT

The disposal of high-level radioactive waste (HLW) in deep geological repository requires reliable data including the solubility and speciation of americium and other actinides in safety assessment. In this work, a generic thermodynamic equilibrium model using the geochemical codes PHREEQC-3 and PhreePlot was used to investigate the solubility of americium in the groundwaters of Beishan in the possible ranges of pH (6–11) and P_{CO2} ($10^{-5.5}$ - $10^{-2.5}$ bar). The pH-logP_{CO2} diagram of solid phases and aqueous species of Am was computed and plotted with Am solubility contour lines. The results indicate that the solubility of Am under the repository far-field conditions is dependent on pH and under the near-field conditions on pH and P_{CO2}. Based on our calculations, we have determined that $AmCO_3OH{\cdot}0.5H_2O(cr)$ is thermodynamically stable in both the near- and far-field conditions, leading to an Am solubility of 4.0×10^{-9} mol/kg and 1.5×10^{-8} mol/kg under, respectively, the near- and far-field conditions of the proposed Beishan repository. However, the amorphous $AmCO_3OH$(*am, hyd*) phase, while thermodynamically metastable, is expected to persist for an extended period of time, possibly hundreds of years or more after the closure of a repository. As such, it is assumed to be the solid phase that limits the solubility of americium, leading to much enhanced Am solubilities of 6.3×10^{-7} and 2.4×10^{-6} mol/kg for the Beishan near- and far-field conditions, respectively. Therefore, solely based on the solubility data, Am could be more toxic than the natural uranium in the Beishan granitic groundwater within ~5000 years after the proposed repository's closure. It is thus important to ensure that Am is well contained by the engineered barriers within this timeframe. Since Am solubilities in Beishan groundwater are rather low, the effect of sorption and colloidal formation could be potentially more important for Am migration in groundwaters, however further studies are required before these processes can be properly evaluated.

1. Introduction

As a major radionuclide in spent nuclear fuels (SNF), Americium (Am) is perhaps one of the least studied actinides with a large inventory worldwide. In addition, Am is a major concern in nuclear material storage and environmental contamination at the legacy sites engaged in nuclear weapons programs, e.g., in Hanford (Zachara et al., 2007; Cantrell and Felmy, 2012; Emerson et al., 2022), in Mayak (Novikov et al., 2009) and in Sellafield (Maher et al., 2016). Am-241 and the other radionuclides in the 4n+1 series including Np-237 emit alpha and beta particles and gamma rays that can pose a significant risk to human if enough is ingested or inhaled. Am-241 can stay in the body for decades, continuing to damage tissues with energetic alpha radiations (Winberg and Garcia, 1995), which will increase a person's chance of developing cancers (Siegel and Bryan, 2003). Therefore, as a man-made element Am can make a significant impact to the environment and be potentially hazardous to the human-being (Siegel and Bryan, 2003; Pusch et al., 2018).

Presently a scientific consensus has been reached worldwide: deep geological repository (DGR) provides a safe disposal for high-level radioactive waste (HLW) permanently (McCartin, 2020). It has been well established that the radioactivity of SNF, i.e., usually the principal component of HLW, is mainly due to the short-lived radionuclides Sr-90 and Cs-137 during the initial several hundred years after creation, due to

* Corresponding author. College of Earth Sciences, Chengdu University of Technology, Chengdu, 610059, China.
E-mail address: pujing.pan@outlook.com (P. Pan).

https://doi.org/10.1016/j.apgeochem.2023.105650
Received 12 November 2022; Received in revised form 16 March 2023; Accepted 30 March 2023
Available online 5 April 2023
0883-2927/© 2023 Elsevier Ltd. All rights reserved.

Am-241 after ~300 up to ~5000 years, and then due to Pu-240, Pu-239, Am-243 and Tc-99. Finally, after ~200,000 years, a mixture of U-238 and Np-237 and their progenies will dominate the remaining small amount of radioactivity - well below that of the natural uranium ores (Siegel and Bryan, 2003). It is estimated that when the proposed China's geological repository is open for loading, there will be 9.58 t Am in the nation's HLW inventory, and after 1000 y of its closure, there will be 4.29 t left (Duan et al., 2021). It is therefore particularly important to understand with high confidence the geochemical characteristics of Am-241 (and the other radionuclides) in a time range of hundreds to tens of thousands of years after a repository's closure, in order to understand its mobility and migration pathway and mechanism for the safety assessment of a geological disposal facility.

While general discussions on the mobility of radionuclides under geological disposal conditions are useful, only the geochemical model calculations based on the site-specific parameters can provide a reliable basis for the evaluation of the source term concentration (maximum solubility) of radionuclides in the near-field and far-field environments of a repository (Wanner, 2007), and in fact this is a regulatory requirement (Birkholzer et al., 2012). In the event that all the engineered barriers of a repository fail prematurely, for instance in <5000 y after closure, Am-241 would be the dominant radioactivity contributor in this scenario, and it could migrate through the geosphere, and possibly, to the biosphere. The migration of Am is governed by a range of geochemical processes, such as solid phase dissolution, speciation, sorption, and colloidal formation. These processes, in turn, are jointly determined by intrinsic characteristics of Am, including its atomic structure and radiochemistry, as well as environmental conditions, including pH, Eh, and groundwater composition.

The radionuclides derived from HLW can only migrate through the geological formations in dissolved aqueous forms. When the water-solid system is in equilibrium, the maximum concentration of a radionuclide in water is determined by the surrounding chemical conditions and is referred to as the 'solubility limit'. One of the key issues in understanding the geochemical processes governing the migration of Am and the other radionuclides under repository conditions is the determination of the solubility limiting solid phase (SLSP). Presently, $Am_2(CO_3)_3(s)$ and $AmOHCO_3(s)$ are generally believed to be the SLSPs in typical repository groundwaters (Silva et al., 2012; Guillaumont and Mompean, 2003), however a recent study shows that the ternary compound $NaAm(CO_3)_2{\cdot}nH_2O(s)$ is stable in natural marine environment (Maloubier et al., 2015), and $NaAm(CO_3)_2{\cdot}5H_2O(cr)$ was believed to be a potential SLSP for Am in place of $AmCO_3OH(am, hyd)$ at the Mol site in Belgium (Wang, 2022). Will the ternary solid-phase be stable under the proposed China's Beishan repository conditions? If the answer is yes, how will the ternary phase affect the solubility of Am in the groundwater in Beishan? These are among the questions that the current paper will address.

Substantial solubility and speciation studies on Am and other actinides in aqueous media have been previously reported in the literature (Guillaumont and Mompean, 2003; Silva et al., 2012; Altmaier and Vercouter, 2012; Altmaier et al., 2013; Wang et al., 2017; Grenthe et al., 2020). The goal of this study is to provide the best-predicted solubility and speciation of Am under the proposed China's deep geological repository conditions for the safety assessment of the Beishan HLW disposal site. Our model and calculations also illustrate the influence of pH and P_{CO2} on the stability of Na-Am-CO_3 phases in the ranges potentially encountered at the Beishan disposal site.

2. Groundwater composition and calculation basis

2.1. China's underground laboratory (URL) and proposed HLW repository

After an initial screening started in 1985 of 21 candidate sites across the entire country, with the local government approval, the Beishan area in northern Gansu Province has emerged as the most appropriate site to construct the first repository for HLW in China (Wang, 2010). Within the general Beishan area which is located in the arid Gobi Desert, five sub-areas corresponding to four granitic intrusions have been identified as potential geological bodies for a repository; the Xinchang site has been selected as the preferred location with the Shazaoyuan site as the backup (Wang et al., 2018). The locations of Xinchang and Shazaoyuan together with some better-known geographical landmarks are shown in Fig. 1.

To systematically develop the technologies necessary for the design, construction and operation of a DGR and experimentally test and verify the pertinent concepts and assumptions, China has decided to construct an underground research laboratory (URL) specifically at or near the proposed Xinchang DGR site with a designed maximum depth of 560 m (Wang et al., 2018). The URL is designed to allow it to become part of the future DGR in terms of capacity, logistics and ventilation requirements. It is currently under construction in full-swing and will soon be used to conduct full-scale experiments in order to better understand the geology, hydrogeology, geochemistry and geo-mechanical conditions of the host rocks (Wang et al., 2018).

2.2. Groundwater compositions

The recently drilled borehole BS28 is adjacent to the under-construction URL as well as the proposed China's first DGR. The water sample from BS28 at a depth of 500 m is a good representation of the Xingchang granitic groundwater (Yang et al., 2019). The carbonate concentration in the Xingchang groundwater is relatively high (2.15×10^{-3} mol/kg), using Henry's law P_{CO2} can be obtained to be $10^{-2.77}$ bar. This water represents the Beishan granitic groundwater before any disturbance and can be regarded as the far-field groundwater with respect to the proposed DGR, and its composition is listed in the second column of Table 1, where the pH and E_h were measured in-situ at a depth of 365–690 m by Yang et al. (2019).

The chemistry of the proposed Beishan DGR groundwater (i.e., the near-field groundwater) is more complex, as the area groundwater will interact with the vitrified HLW, the metal containers, and the buffer and backfill materials. In the laboratory, the Beishan granite porewater was used to react with the Gaomiaozi Na-bentonite (i.e., the proposed China's DGR backfill/buffer material) and a low-carbon steel (a candidate packaging container material) successively (Lu et al., 2015; Wei

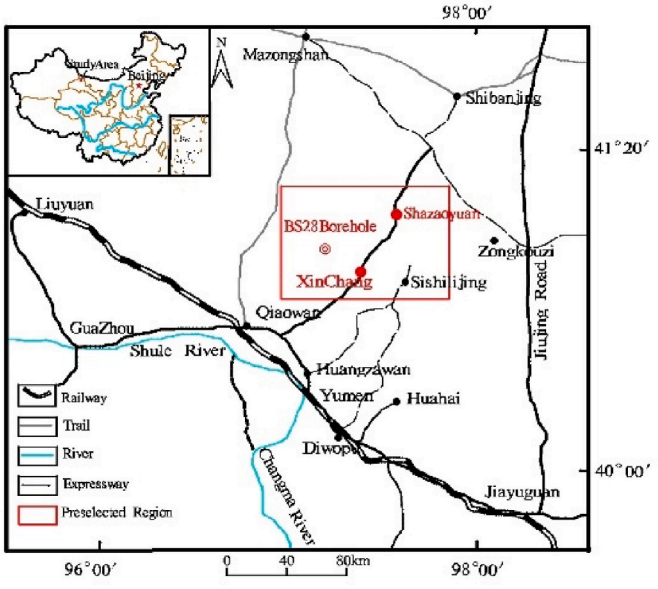


Fig. 1. Location of the study area, with Borehole 28 and the sub-areas Xingchang and Shazaoyuan shown.

Table 1
Chemical compositions of groundwaters in the Beishan study area (mol/kg).

	Vault (near-field) water[a]	BS28 (far-field) water[b]
Na+	3.23×10^{-2}	4.52×10^{-2}
Ca^{2+}	3.42×10^{-4}	4.58×10^{-3}
K^{+}	1.16×10^{-4}	4.09×10^{-4}
Mg^{2+}	1.19×10^{-4}	2.08×10^{-3}
Cl^{-}	1.79×10^{-2}	3.62×10^{-2}
HCO_3^{-}	2.31×10^{-3}	2.15×10^{-3}
SO_4^{2-}	1.15×10^{-4}	9.18×10^{-3}
F^{-}	–	1.06×10^{-4}
NO_3^{-}	3.67×10^{-4}	2.28×10^{-4}
SiO_2(aq)	7.05×10^{-5}	9.12×10^{-5}
pH	8.9	7.8
E_h	−182 (mV)	98 (mV)

- not reported.
[a] Derived from Lu et al. (2015) and Wei et al. (2019).
[b] Derived from Yang et al. (2019) and Guo et al. (2014).

et al., 2019). The resulting water may be regarded as the near-field repository groundwater (vault water), and its composition is listed in the first column of Table 1. It is expected that the near-field groundwater would be more oxidizing relative to the far-field condition because of the ingression of the atmospheric air to the vault during construction; however, experiments (Lu et al., 2015; Wei et al., 2019) have shown that the near-field groundwater would be more reducing than the undisturbed far-field groundwater (−182 mV vs. 98 mV). This reducing effect may be attributed to the presence of the reducing minerals including pyrite (impurity in bentonite) and elemental iron (stainless steel) and the small amounts of cellulose, plastic and rubber (CPR) matter.

As shown in Table 1, both the Beishan near-field and far-field groundwaters are of the SO_4^{2-}-Cl^{-}-Na^{+} type. Extensive grouting with low-alkali cement during the DGR construction and closure may be needed. The degradation of the low-alkali cement may cause groundwater pH to shift in the range of 6–11, the adsorption coefficient data (K_d) currently in use for DGR safety assessment are valid within this pH range (Andersson et al., 2000). If magnesium oxide (MgO(s)) is added to the engineered barriers for pH and carbonate concentration control, P_{CO2} in the repository would be reduced from $10^{-2.5}$ bar to $10^{-5.5}$ bar (Schramke et al., 2020). Below, we will discuss how changes in pH and P_{CO2} in the near-field, as well as changes in pH in the far-field, could impact the solubility of Am in the Beishan groundwaters.

2.3. Thermodynamic data

The geochemical code PHREEQC-3 (and PhreePlot, a code based on PHREEQC with extensive charting capability, Kinniburgh and Cooper, 2011) made available by the United States Geological Survey (USGS) (Parkhurst and Appelo, 2013), was used for carrying out the simulations in this work. A known limitation of the software is the lack of internal consistency in the databases supplied with the software (Parkhurst and Appelo, 2013). Therefore, it is necessary to first carefully evaluate all the available thermodynamic data of the components involved in our calculations.

The Nuclear Energy Agency Thermodynamic Data Base (NEA-TDB) project, sponsored by the Organization for Economic Cooperation and Devourment (OECD), was specifically established to create an internally consistent high-quality thermodynamic database of relevant elements to meet the modeling requirement for safety assessment of radioactive waste disposal systems (Östhols and Wanner, 2000). Therefore, in this work most of the thermodynamic data used were taken from the recent NEA-TDB publication (Grenthe et al., 2020), where the relevant thermodynamic data for U, Np, Pu, Am and Tc were rigorously reassessed and the appropriate updates were recommended, as listed in Table 2.

Although Am can be found in +3, +4, +5 and + 6 oxidation states in natural environments, in the Beishan groundwater with an E_h ranging from approximately −200 mV – 100 mV, only the +3 oxidation state is stable (Vercouter et al., 2004). Am exists in the +4 state only when Am (IV) is stabilized by strong complexes, Am(V) is prone to disproportionation and reduction, and Am(VI) can only be stabilized under highly oxidizing conditions (Grenthe et al., 2020). As a result, this study considers only the aqueous species and solid compounds of Am(III) in its calculations.

2.3.1. Solubility-limiting solid phases (SLSP)

The NEA-TDB recently recommended database contains the data for the 7 solid phases of Am(III) including 3 amorphous and 4 crystalline phases (Grenthe et al., 2020), i.e., $Am(OH)_3$ (am), $Am_2(CO_3)_3$ (am), $AmCO_3OH$(am, *hyd*), Am_2O_3(cr), $Am(OH)_3$ (cr), $AmCO_3OH{\bullet}0.5H_2O$

Table 2
The formation constants and other thermodynamic data of aqueous species and solid compounds of Am(III) used in this work (Grenthe et al., 2020).

Aqueous species	Reactions	LogK	$\Delta_f G°/(kJ{\bullet}mol^{-1})$	$\Delta_f H°/(kJ{\bullet}mol^{-1})$	$\Delta_f S°/(kJ{\bullet}mol^{-1})$
$AmOH^{2+}$	$Am^{3+} + H_2O \rightleftharpoons AmOH^{2+} + H^{+}$	−7.200 ± 0.500	41.098 ± 2.854		
$Am(OH)_2^{+}$	$Am^{3+} + 2H_2O \rightleftharpoons Am(OH)_2^{+} + 2H^{+}$	−15.100 ± 0.700	86.191 ± 3.996		
$Am(OH)_3$ (aq)	$Am^{3+} + 3H_2O \rightleftharpoons Am(OH)_3$ (aq) + $3H^{+}$	−26.200 ± 0.500	149.551 ± 2.854		
AmF^{2+}	$Am^{3+} + F^{-} \rightleftharpoons AmF^{2+}$	3.400 ± 0.400	−19.407 ± 2.283	12.100 ± 2.200	105.675 ± 10.634
AmF_2^{+}	$Am^{3+} + 2\,F^{-} \rightleftharpoons AmF_2^{+}$	5.800 ± 0.200	−33.107 ± 1.142	45.100 ± 14.500	262.308 ± 48.784
$AmCl^{2+}$	$Am^{3+} + Cl^{-} \rightleftharpoons AmCl^{2+}$	0.240 ± 0.350	−1.370 ± 2.000		
$AmCl_2^{+}$	$Am^{3+} + 2\,C\,l^{-} \rightleftharpoons AmCl_2^{+}$	−0.810 ± 0.350	4.624 ± 1.998	54.900 ± 4.500	168.627 ± 16.514
$AmSO_4^{+}$	$Am^{3+} + SO_4^{2-} \rightleftharpoons AmSO_4^{+}$	3.500 ± 0.300	−19.978 ± 1.712	40.000 ± 4.000	201.167 ± 14.593
$Am(SO_4)_2^{-}$	$Am^{3+} + 2SO_4^{2-} \rightleftharpoons Am(SO_4)_2^{-}$	5.000 ± 1.000	−28.540 ± 5.708	70.000 ± 7.000	330.505 ± 30.294
$AmNO_3^{2+}$	$Am^{3+} + NO_3^{-} \rightleftharpoons AmNO_3^{2+}$	1.280 ± 0.0500	−7.306 ± 0.285	1.800 ± 1.000	30.542 ± 3.489
$Am(NO_3)_2^{+}$	$Am^{3+} + 2NO_3^{-} \rightleftharpoons Am(NO_3)_2^{+}$	0.880 ± 0.110	−5.023 ± 0.628	10.800 ± 2.200	53.071 ± 7.674
$AmCO_3^{+}$	$Am^{3+} + CO_3^{2-} \rightleftharpoons AmCO_3^{+}$	8.000 ± 0.400	−45.664 ± 2.283		
$Am(CO_3)_2^{-}$	$Am^{3+} + 2CO_3^{2-} \rightleftharpoons Am(CO_3)_2^{-}$	12.900 ± 0.600	−73.634 ± 3.425		
$Am(CO_3)_3^{3-}$	$Am^{3+} + 3CO_3^{2-} \rightleftharpoons Am(CO_3)_3^{3-}$	15.000 ± 0.500	−85.621 ± 2.854		
$AmHCO_3^{2+}$	$Am^{3+} + HCO_3^{-} \rightleftharpoons AmHCO_3^{2+}$	3.100 ± 0.300	−17.695 ± 1.712		
$AmSiO(OH)_3^{2+}$	$Am^{3+} + SiO(OH)_3^{-} \rightleftharpoons AmSiO(OH)_3^{2+}$	8.130 ± 0.200	−46.406 ± 1.142	18.600 ± 4.000	218.031 ± 13.952
SLSP[a]					
$Am(OH)_3$ (am)	$Am(OH)_3$ (am) + $3H^{+} \rightleftharpoons Am^{3+} + 3H_2O$(l)	16.900 ± 0.800	96.466 ± 4.566		
$Am(OH)_3$ (cr)	$Am(OH)_3$ (cr) + $3H^{+} \rightleftharpoons Am^{3+} + 3H_2O$(l)	15.600 ± 0.600	89.045 ± 3.425		
$Am_2(CO_3)_3$ (am)	$Am_2(CO_3)_3$ (am) $\rightleftharpoons 2Am^{3+} + 3CO_3^{2-}$	−33.400 ± 2.200	190.649 ± 12.558		
$AmCO_3OH$(am,hyd)	$AmCO_3OH$(am,hyd) $\rightleftharpoons Am^{3+} + CO_3^{2-} + OH^{-}$	−20.200 ± 1.000	115.302 ± 5.708		
$AmCO_3OH{\cdot}0.5H_2O$(cr)	$AmCO_3OH{\cdot}0.5H_2O$(cr) $\rightleftharpoons Am^{3+} + CO_3^{2-} + 0.5H_2O$(l) + OH^{-}	−22.400 ± 0.500	127.860 ± 2.854		
$NaAm(CO_3)_2{\cdot}5H_2O$(cr)	$NaAm(CO_3)_2{\cdot}5H_2O$(cr) $\rightleftharpoons Am^{3+} + 5H_2O$(l) + $2CO_3^{2-} + Na^{+}$	−21.000 ± 0.500	119.869 ± 2.854		
Am_2O_3(cr)	Am_2O_3(cr) + $6H^{+} \rightleftharpoons 2Am^{3+} + 3H_2O$(l)	53.120 ± 5.030	−303.266 ± 28.714		

[a] Solubility limiting solid phase.

(cr), and $NaAm(CO_3)_2{\bullet}5H_2O$(cr). The thermodynamic data and geochemical behavior of the binary Am-OH and Am-CO_3 solid phases have been discussed in many published studies (Altmaier and Vercouter, 2012; Altmaier et al., 2013; Guillaumont and Mompean, 2003; Silva et al., 2012). The thermodynamic data for the ternary solid phase $NaAm(CO_3)_2{\bullet}5H_2O$(cr), were provided by Vercouter et al. (2004, 2005a; 2005b).

The solid phase $NaAm(CO_3)_2{\cdot}xH_2O$(s) was experimentally characterized by thermogravimetry, infrared (IR) spectroscopy, and X-ray powder diffraction (XRD) analysis, and its comparable solubility values in low carbonate solutions were reported by Meinrath and Kim (1991) and Thoenen et al. (2014). However, Meinrath and Kim (1991) obtained two sets of solubility data with $[CO_3^{2-}] > 10^{-4}$ mol/kg, presumably because of two solids with different crystallinity formed. In an NEA-TDB earlier review (Thoenen et al., 2014), the solid $NaAm(CO_3)_2{\cdot}xH_2O(s)$ (x=5) was already suggested to be accepted with caution, and more experimental work with varying P_{CO2} was called for. Vercouter et al. (2005b) studied the solubility of $NaEu(CO_3)_2{\bullet}5H_2O(cr)$ over a wide range of carbonate concentrations with the solid-phase characterized by the time-resolved laser fluorescence spectroscopy (TRLFS). Because of the chemical similarities between Eu(III) and Am(III), similar solid is also expected for the Am(III)–CO_3 system, and the derived data were recommended by the recent NEA-TDB review (Grenthe et al., 2020). As $Am_2(CO_3)_3$ (am) and $NaAm(CO_3)_2{\bullet}5H_2O$(cr) exist under different CO_2 partial pressures, they were both included in this work.

The amorphous phases are not thermodynamically stable, over time they transform into ordered crystalline solids with lower free energies of formation, hence the reported thermodynamic data in the literature for these amorphous solids are not reliable and in general not suitable for equilibrium calculations. The Am solubility defined by the amorphous $Am(OH)_3$ (am) was reported to be nearly 2 orders of magnitude greater than the crystalline counterpart (Wang et al., 2017). Therefore, Am $(OH)_3$ (cr) rather than $Am(OH)_3$ (am) was included in our initial calculations. As there are no well-defined corresponding crystalline forms reported for $Am_2(CO_3)_3$ (am) and $AmCO_3OH$(am, hyd), these two amorphous solid phases were also included in our initial equilibrium model. However, as we will discuss in greater length later, the dissolved Am or its apparent solubility in groundwaters is likely controlled by the metastable amorphous phases. For this reason, we later included all potentially important americium solid phases in our model calculations.

In fact, it can be an over-simplification of reality to denote an Am-solid either as crystalline or amorphous, because an Am-solid likely always exists in a state between pure crystalline and complete amorphous. This is due to the fact that the strong self-irradiation of α-decays (particularly of Am-241) will damage the crystalline structure over time. The distinction between amorphous and crystalline Am solid in experiment is ambiguous. The bulk structure of an Am-solid may be mostly crystalline based on X-ray diffraction analysis, however its surface may be largely amorphous due to α-radiolysis. As a result, the experimentally determined solubility and the derived thermodynamic data may not accurately reflect the bulk composition, since they are primarily determined by the surface characteristics (Silva et al., 2012). The solubilities of the crystalline actinide compounds can be 2 to 3 orders magnitude lower than those of their amorphous counterparts (Merli and Fuger, 1996), therefore the solubility results based on amorphous substances are conservative estimates for DGR safety assessment. The thermodynamic stability of americium solid phases is not entirely clear, and not all the solubility data are currently available. Additionally, the persistence of each amorphous phase is uncertain. As a result, selecting the appropriate SLSP under a given geochemical environment is not always straightforward. While using only amorphous phases as SLSPs is a safer and more conservative approach, this can lead to grossly incorrect outcomes for longer-lived radionuclides such as Am. This is because the amorphous phase may convert to a crystalline phase with much reduced solubility long before it has decayed away. Hence, in this study we strive to present a complete picture by including all the available data (including the pseudo-thermodynamic data of amorphous Am phases) in our model and calculate Am solubilities in different scenarios.

Based on the discussions above and a review of the literature (e.g., Grenthe et al., 2020; Thoenen et al., 2014; Vercouter et al., 2004; Silva et al., 2012), a sequence of viable solid phases that may control the solubility of Am in groundwaters at different times and under different conditions is desirable. To obtain this sequence, we used a model that predicts the potential formation of a series of minerals by suppressing the more stable/feasible solid phases incrementally. The calculations were performed by equilibrating 1 g of each solid phase with near-field or far-field groundwater. The sequence under the Beishan far-field conditions is the following: 1) $Am(OH)_3$ (*am*) (thermodynamically least table but kinetically favored) → 2) $Am(OH)_3$ (*cr*) → 3) $AmCO_3OH$ (*am, hyd*) → 4) $Am_2(CO_3)_3$ (*am*) → 5) $NaAm(CO_3)_2{\cdot}5H_2O$(*cr*) → 6) $AmCO_3OH{\cdot}0.5H_2O$(*cr*) (thermodynamically stable phase). Under the near-field conditions, due to the elevated P_{CO2} levels the sequence is a little different as: 1) $Am(OH)_3$ (*am*) (least stable) → 2) $Am_2(CO_3)_3$ (*am*) → 3) $AmCO_3OH$ (*am, hyd*) → 4) $NaAm(CO_3)_2{\cdot}5H_2O$(*cr*) → 5) $Am(OH)_3$ (*cr*) → 6) $AmCO_3OH{\cdot}0.5H_2O$(*cr*) (stable). Although the amorphous phases are not thermodynamically stable, all can however exist in natural aquifers for various lengths of time depending on pH, P_{CO2} and the other geochemical conditions. Please note that these sequences obtained are qualitative in nature.

2.3.2. Aqueous complexes of Am(III)

It follows from the previous sections that in addition to the Am(III) hydrolysis reactions, the complexation of Am(III) with fluoride, chloride, nitrate, sulfate and bicarbonate is most likely the main process responsible for Am speciation in Beishan groundwater. To model these processes, the necessary thermodynamic data from Grenthe et al. (2020) were employed. Since silica veins are widely observed in the granitic plutons in the study area (Liu et al., 2007; Tian et al., 2014), the role of Si in the dissolution and speciation of Am and other actinides in the HLW cannot be ignored, Si was therefore included in our calculations. The selected thermodynamic data together with the associated chemical reactions are listed in Table 2.

Using Eu(III) and Nd(III) analogues, Schott et al. (2014) and Hinz et al. (2015) determined, separately, that the precipitation of +3 actinides as borate solids could significantly reduce +3 actinide concentrations in circumneutral to mildly alkaline (pH up to 9) solutions. On the other hand, Borkowski et al. (2010) found that total boron concentrations up to 0.16 mol/L increased Nd(III) solubilities in solutions up to 5 mol/L NaCl. More recently, Xiong et al. (2017) investigated the effect of high borate concentrations (~0.5 mol/kg) in 0.01 and 0.1 mol/kg NaCl solutions on the solubility of Am(III), using Nd(III) as an analogue. They found that borate can enhance the solubility of $Nd(OH)_3$ (micro cr) at such high borate concentrations. In China's HLW disposal strategy, the waste will be vitrified into a borosilicate glass matrix before loading. As a result, boron could be an important factor in the safety assessment of HLW disposal. However, no thermodynamic data for the Am-borate reactions were recommended in the most recent NEA-TDB review (Grenthe et al., 2020), so the impact of Am(III) complexation with boron will need to be evaluated in future studies.

While the existence of some ternary Ca-Am-OH complexes has been suggested, which could enhance the solubility of Am(III) in high calcium brines (Rabung et al., 2008; Neck et al., 2009), no thermodynamic data for such complexes were included in the most recent NEA-TDB review (Grenthe et al., 2020). Moreover, this type of complexes only forms in highly concentrated $CaCl_2$ solutions, which are not relevant to the present study. Therefore, our model does not include these complexes.

The ionic strength effect on the Am(III) complex formation constants was treated using the Davies equation as implemented in PHREEQC-3 (Parkhurst and Appelo, 2013).

3. Results and discussion

3.1. Am solubility under Beishan far-field conditions

It is assumed that after the loading is completed and the geological disturbances to the host rocks have finally subsided, the groundwater at depth surrounding a DGR will gradually return to the original state as before excavation. In Beishan, the far-field groundwater can be represented by the recently sampled water from the BS28 borehole at a depth of 500 m (Yang et al., 2019), as presented in Table 1. Under such assumed far-field conditions, our calculations show that the solubility of Am would be 1.5×10^{-8} mol/kg and the main aqueous Am species would be $AmCO_3^+$(52%), $AmSiO(OH)_3^{2+}$(24%) and $Am(CO_3)_2^-$(20%), with the thermodynamically stable phase $AmCO_3OH{\cdot}0.5H_2O(cr)$ being the SLSP. Jiang et al. (2014), using their self-developed software CHEMSPEC, estimated that the solubility of Am in the Beishan groundwater was 2.01×10^{-7} mol/kg (pH = 7.56, E_h = 164 mV, $[HCO_3^-] = 2.15 \times 10^{-3}$ mol/kg), which is in fair agreement with our result given the differences in pH values used (while E_h would not have direct impact).

Some experiments on Am solubility in organic-free solutions have been conducted by various research groups (Berner, 2014; Bruggeman et al., 2012; Trofimov et al., 2008; Zhou et al., 2015). Zhou et al. (2015) performed their work using a synthesized solution ($NaHCO_3$–$NaSO_4$–NaCl as background electrolytes, pH = 8.3, $[HCO_3^-] = 8.0 \times 10^{-4}$ mol/kg, and total $[Am^{3+}] = 1.0 \times 10^{-6}$ mol/kg) similar to the Beishan groundwater without organic matter, and found Am solubility to be 8.20×10^{-10} mol/kg after ultrafiltration at 3 kD. The resulting solid phase was not characterized. By using their solution composition and our calculation methodology, we obtained the Am solubility of 3.0×10^{-9} mol/kg for their synthetic Beishan groundwater, with $AmCO_3OH{\cdot}0.5H_2O(cr)$ being the solid phase, and $AmCO_3^+$(66%) and $Am(CO_3)_2^-$(29%) being the dominant aqueous species. The measured Am solubility from the synthesized solution of Zhou et al. (2015) is almost 4 times lower when compared to our calculated result using the equilibrium model. Based on the work of Maes et al. (2004), we believe that the discrepancy can be attributed to the leakage of CO_2(g) during the experiment of Zhou et al. (2015). In the experiment of Zhou et al. (2015), P_{CO2} was not maintained throughout, which may have led to the leakage of CO_2(g). As a result, an early-formed Am–OH–CO_3 solid phase may have converted to an Am-OH solid phase, ultimately causing a decrease in Am solubility.

The main factors affecting the solubility of Am under DGR conditions include pH, P_{CO2} and E_h (Wang, 2022). As discussed earlier, +3 is practically the only stable valence state of Am in the natural environment, and Am(V) exists only in extremely oxidizing environments (Altmaier et al., 2013; Altmaier and Vercouter, 2012; Guillaumont and Mompean, 2003; Grenthe et al., 2020; Silva et al., 2012) which is unlikely the case in either near-field or far-field of Beishan DGR. Therefore, the main factors affecting the solubility of Am are pH and P_{CO2}. The far-field condition is assumed to be a hardly disturbed reducing environment and P_{CO2} would not fluctuate greatly, therefore only the impact of pH change to the solubility and speciation of Am(III) in the far-field groundwater was evaluated and the results are shown in Table 3 and Fig. 2.

Fig. 2 illustrates the dominance of different aqueous Am(III) species under Beishan far-field conditions at varying pH values. At pH 6, the main Am(III) species in solution are $AmSO_4^+$ and Am^{3+}. As pH increases to 7, $AmSiO(OH)_3^{2+}$ becomes the dominant species, followed by $AmCO_3^+$ at pH 7.5. Only when pH approaching 8.5, $Am(CO_3)_3^{3-}$ and $Am(CO_3)_2^-$ become the principal species. The solubility of Am remains relatively constant between pH 6 and 10, with a notable decrease around pH 8.

The saturation indices of the two crystalline Am solid phases $AmCO_3OH{\cdot}0.5H_2O(cr)$ and $NaAm(CO_3)_2{\bullet}5H_2O(cr)$ as a function of pH under the far-field conditions are shown in Fig. 3. The results indicate that at a pH just beyond 9.5, there is a solid phase transition from $AmCO_3OH{\cdot}0.5H_2O(cr)$ to $NaAm(CO_3)_2{\bullet}5H_2O(cr)$, i.e., $AmCO_3OH{\cdot}0.5H_2O(cr)$ starts to dissolve meanwhile NaAm(CO3)2•5H2O(cr) begins to precipitate out of solution. Apparently, $AmCO_3OH{\cdot}0.5H_2O(cr)$ is expected to be the stable solid phase in the far-field of Beishan DGR under normal circumstances (pH = ~7.8) assuming dissolution equilibrium is reached.

Table 3
Solubility and speciation of Am in Beishan far-field conditions at different pHs (25 °C and $P_{CO2} = 10^{-2.77}$ bar).

pH	Solubility (mol/kg)	Solid phase	Main Species (%)
6	8.2×10^{-5}	$AmCO_3OH{\cdot}0.5H_2O$ (cr)	$AmSO_4^+$(48); Am^{3+}(29); $AmSiO(OH)_3^{2+}$(15)
6.5	3.8×10^{-6}	$AmCO_3OH{\cdot}0.5H_2O$ (cr)	$AmSiO(OH)_3^{2+}$(37); $AmSO_4^+$(33); Am^{3+}(19)
7	2.7×10^{-7}	$AmCO_3OH{\cdot}0.5H_2O$ (cr)	$AmSiO(OH)_3^{2+}$(54); $AmCO_3^+$(18); $AmSO_4^+$(15); Am^{3+}(9)
7.5	3.4×10^{-8}	$AmCO_3OH{\cdot}0.5H_2O$ (cr)	$AmCO_3^+$(45); $AmSiO(OH)_3^{2+}$(42)
8	1.1×10^{-8}	$AmCO_3OH{\cdot}0.5H_2O$ (cr)	$AmCO_3^+$(44); $Am(CO_3)_2^-$(42); $AmSiO(OH)_3^{2+}$(13)
8.5	1.8×10^{-8}	$AmCO_3OH{\cdot}0.5H_2O$ (cr)	$Am(CO_3)_2^-$(83); $AmCO_3^+$(9); $Am(CO_3)_3^{3-}$(8)
9	1.0×10^{-7}	$AmCO_3OH{\cdot}0.5H_2O$ (cr)	$Am(CO_3)_3^{3-}$(53); $Am(CO_3)_2^-$(47)
9.5	9.2×10^{-7}	$NaAm(CO_3)_2{\bullet}5H_2O$ (cr)	$Am(CO_3)_3^{3-}$ (95); $Am(CO_3)_2^-$(5)
10	3.9×10^{-10}	$NaAm(CO_3)_2{\bullet}5H_2O$ (cr)	$Am(CO_3)_2^-$(100)

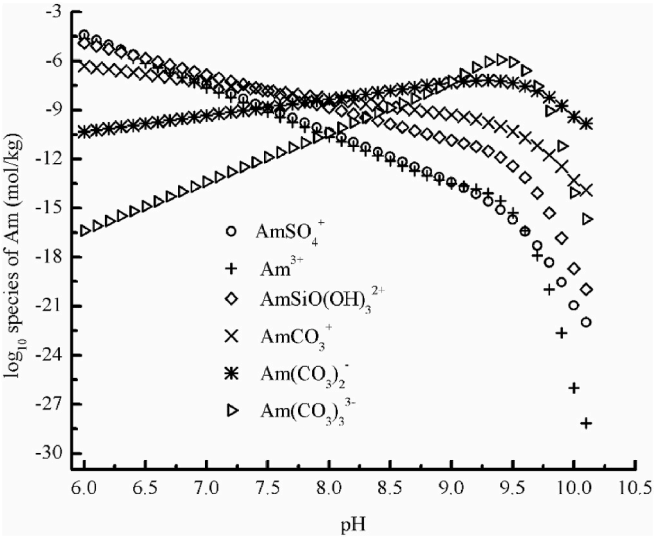


Fig. 2. Equilibrium aqueous Am(III) species concentration vs. pH under Beishan far-field conditions (25 °C and $P_{CO2} = 10^{-2.77}$ bar).

3.2. Am solubility under Beishan near-field conditions

The chemistry of the groundwater of the proposed Beishan DGR (i.e., the near-field groundwater) is anticipated to be considerably more complex than that of the far-field conditions. This is because the local groundwater will undergo intricate interactions with the vitrified HLW (the planned waste form, Wang et al., 2018), the metal containers, and the buffer and backfill materials, starting from the initial placement of the HLW canisters. In order to have a reasonable assessment of the geochemical processes after the closure of the proposed DGR, the Beishan granitic porewater was used in experiments to react with the various engineering barrier materials successively (Lu et al., 2015; Wei et al., 2019), the resulting water can be regarded as the repository vault

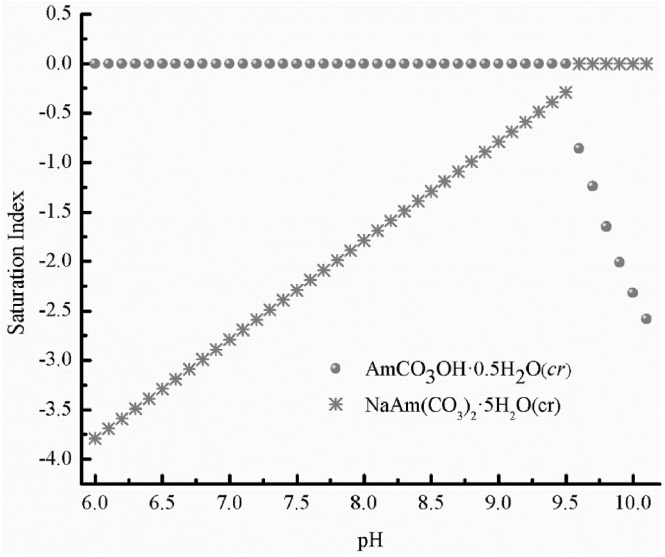


Fig. 3. Saturation indices of $AmCO_3OH{\cdot}0.5H_2O(cr)$ and $NaAm(CO_3)_2{\bullet}5H_2O(cr)$ over the pH range 6–11 under the Beishan far-field conditions (25 °C and $P_{CO2} = 10^{-2.77}$ bar).

water, i.e., groundwater under the near-field conditions (Column 1 of Table 1).

After the repository is closed, the remaining oxygen is expected to be depleted quickly, leading to a reduced environment with an E_h of −182 mV, as reported by Lu et al. (2015) and Wei et al. (2019). At the same time, the pH of the groundwater is expected to increase from its natural value of around 8 to a more basic value of around 9, due to the degradation of the grouting. Additionally, if MgO(s) is added to the buffer and backfill materials, the P_{CO2} in the groundwater is expected to decrease. As the granite repository is highly stable and little groundwater recharges would be expected, our model of the near-field environment is simply assumed to be a closed cave filled with the NaCl–$NaSO_4$ groundwater. Changes in the solubility of Am under the conditions of potential pH (6–11) and P_{CO2} ($10^{-5.5}$ - $10^{-2.5}$ bar) ranges have been evaluated, the results are presented in Table 4 and Fig. 4. It should be noted that when pH exceeds 10, the system becomes unstable at high P_{CO2} levels ($P_{CO2} > 10^{-3.5}$ bar) and no meaningful results could be obtained using PHREEQC-3.

The calculated main species of Am(III) at different P_{CO2} and pH under the repository near-field conditions are also given in Table 4. The Am solubility specifically corresponding to the near-field conditions (Table 1) is 4.0×10^{-9} mol/kg and the main aqueous Am species would be $Am(CO_3)_2^-$(78%) and $AmCO_3^+$(15%), with $AmCO_3OH{\cdot}0.5H_2O(cr)$ being the SLSP. It is worth noting that increasing P_{CO2} leads to a decrease in Am solubility. This suggests that Am(III) dissolves in water primarily through hydrolysis, and that dissolved carbonate competes with Am (III)–OH^- complexes for hydroxyl ions. At different P_{CO2}, the total dissolved carbonate in solution is shown as a function of pH in Fig. 4 (right). At $P_{CO2} = 10^{-2.5}$ bar, the solubility of Am decreases to a minimum as pH increases from 6 to ~7.75, and then increases until reaching a maximum at pH ~8.75. As pH continues to increase, Am solubility sharply decreases again. The trend is also noted at lower P_{CO2} values ($P_{CO2} = 10^{-3.5}$, $10^{-4.5}$, and $10^{-5.5}$ bar), but with the solubility curves gradually shifting toward higher pH values (Fig. 4). In the pH and P_{CO2} ranges of interest (pH = 6–11 and $P_{CO2} = 10^{-5.5}$ - $10^{-2.5}$ bar), the highest Am solubility (2.8×10^{-2} mol/kg) occurs in an acidic solution (pH 6) with the lowest P_{CO2} ($10^{-5.5}$ bar), with the solid phase being $AmCO_3OH{\cdot}0.5H_2O(cr)$. Conversely, the lowest solubility (7.5×10^{-11} mol/kg) is observed in an alkaline solution with the highest P_{CO2} ($10^{-2.5}$ bar), with the solid phase being $NaAm(CO_3)_2{\bullet}5H_2O(cr)$. It appears that increasing P_{CO2} tends to dampen the impact of pH change on the dissolved amount of Am in aqueous solutions (see Fig. 4).

From Table 4, it is also noted that the solid phase $NaAm(CO_3)_2{\bullet}5H_2O$ (*cr*) is stable only when $\log P_{CO2} \geq -4.5$ bar and pH ≥ 9, this is consistent with the work of Vercouter et al. (2005a, 2005b) who observed that when $NaAm(CO_3)_2$ (*cr*) was used as the SLSP in their experiments, Am solubility was reduced and there was a large amount of CO_3^{2-} in the solution. Vercouter et al. (2004) reviewed the experimental results of Giffaut (1994) and concluded that when $NaAm(CO_3)_2$(s) was used in Am solubility experiments, the dominant species in solution were $Am(CO_3)_i^{3-2i}$ (i = 1–3), that is also in agreement with our results (Table 4). It is worth noting that under the Beishan DGR near-field conditions, $AmCO_3OH{\bullet}0.5H_2O(cr)$ is the stable solid phase; $NaAm(CO_3)_2{\bullet}5H_2O(cr)$

Table 4
Solubility of Am in Beishan near-field groundwater with varying pH and P_{CO2} values ($E_h = -182$ mV, T = 25 °C).

pH	Solubility (mol/kg)	Solid phase	Major Species (%)	Solubility (mol/kg)	Solid phase	Major Species (%)
	$\log P_{CO2} = -2.5$ bar			$\log P_{CO2} = -3.5$ bar		
6.0	1.4×10^{-5}	$AmCO_3OH{\bullet}0.5H_2O$ (cr)	Am^{3+}(59); $AmSiO(OH)_3^{2+}$(34)	1.4×10^{-4}	$AmCO_3OH{\bullet}0.5H_2O$ (cr)	Am^{3+}(71); $AmSiO(OH)_3^{2+}$(25)
7.0	1.1×10^{-7}	$AmCO_3OH{\bullet}0.5H_2O$ (cr)	$AmSiO(OH)_3^{2+}$(44); $AmCO_3^+$(44); Am^{3+}(7)	6.0×10^{-7}	$AmCO_3OH{\bullet}0.5H_2O$ (cr)	$AmSiO(OH)_3^{2+}$(76); Am^{3+}(12);
8.0	1.4×10^{-8}	$AmCO_3OH{\bullet}0.5H_2O$ (cr)	$Am(CO_3)_2^-$(61); $AmCO_3^+$ (34)	1.0×10^{-8}	$AmCO_3OH{\bullet}0.5H_2O$ (cr)	$AmCO_3^+$ (44); $AmSiO(OH)_3^{2+}$(44); $Am(CO_3)_2^-$(8)
9.0	2.9×10^{-7}	$NaAm(CO_3)_2{\bullet}5H_2O$ (cr)	$Am(CO_3)_3^{3-}$(69); $Am(CO_3)_2^-$(31)	9.6×10^{-9}	$AmCO_3OH{\bullet}0.5H_2O$ (cr)	$Am(CO_3)_2^-$(86); $Am(CO_3)_3^{3-}$(9)
10.0	7.5×10^{-11}	$NaAm(CO_3)_2{\bullet}5H_2O$ (cr)	$Am(CO_3)_2^-$(100)	9.4×10^{-7}	$NaAm(CO_3)_2{\bullet}5H_2O$ (cr)	$Am(CO_3)_3^{3-}$(97)
	$\log P_{CO2} = -4.5$ bar			$\log P_{CO2} = -5.5$ bar		
6.0	1.1×10^{-3}	$AmCO_3OH{\bullet}0.5H_2O$ (cr)	Am^{3+}(90); $AmSiO(OH)_3^{2+}$(6)	2.8×10^{-2}	$AmCO_3OH{\bullet}0.5H_2O$ (cr)	Am^{3+}(97)
7.0	6.3×10^{-6}	$AmCO_3OH{\bullet}0.5H_2O$ (cr)	$AmSiO(OH)_3^{2+}$(81); Am^{3+}(13)	3.8×10^{-5}	$AmCO_3OH{\bullet}0.5H_2O$ (cr)	$AmSiO(OH)_3^{2+}$(74); Am^{3+}(19)
8.0	6.2×10^{-8}	$AmCO_3OH{\bullet}0.5H_2O$ (cr)	$AmSiO(OH)_3^{2+}$(83); $AmCO_3^+$ (9)	5.0×10^{-7}	$AmCO_3OH{\bullet}0.5H_2O$ (cr)	$AmSiO(OH)_3^{2+}$(90); $Am(OH)_2^+$(4)
9.0	2.0×10^{-9}	$AmCO_3OH{\bullet}0.5H_2O$ (cr)	$Am(CO_3)_2^-$(44); $AmCO_3^+$(25); $AmSiO(OH)_3^{2+}$(21) $Am(OH)_2^+$(9)	6.3×10^{-9}	$AmCO_3OH{\bullet}0.5H_2O$ (cr)	$AmSiO(OH)_3^{2+}$(62); $Am(OH)_2^+$(26); $AmCO_3^+$(7)
10.0	2.3×10^{-8}	$AmCO_3OH{\bullet}0.5H_2O$ (cr)	$Am(CO_3)_3^{3-}$(62); $Am(CO_3)_2^-$(38)	1.1×10^{-9}	$AmCO_3OH{\bullet}0.5H_2O$ (cr)	$Am(CO_3)_2^-$(72); $Am(OH)_2^+$(14); $Am(CO_3)_3^{3-}$(7)
11.0	7.7×10^{-11}	$NaAm(CO_3)_2{\bullet}5H_2O$ (cr)	$Am(CO_3)_2^-$(100)	3.3×10^{-7}	$AmCO_3OH{\bullet}0.5H_2O$ (cr)	$Am(CO_3)_3^{3-}$(97)

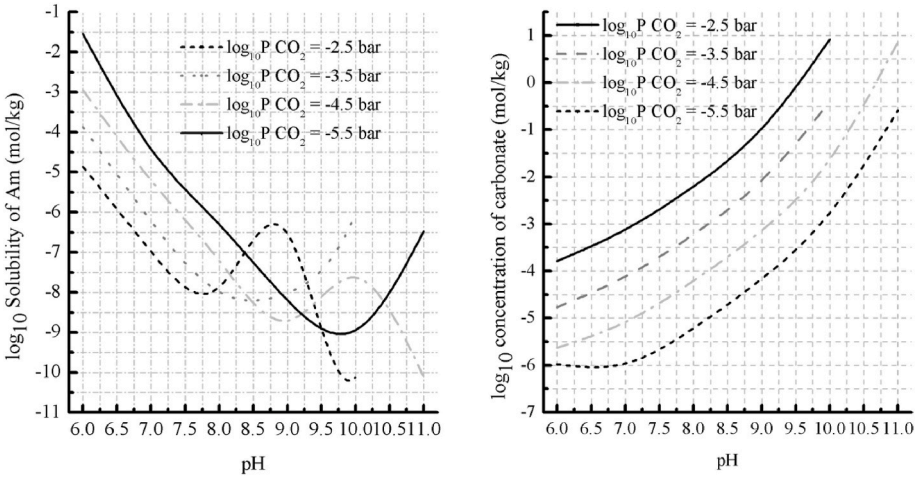


Fig. 4. Left, influence of pH and P_{CO2} on the solubility of Am at Beishan near-field conditions (E_h = −182 mV, T = 25 °C). Right, total carbonate vs. pH at different P_{CO2}.

is stable only in basic solutions (pH > 9) with relatively high level of CO_2 ($logP_{CO2} > -4.5$ bar).

3.3. Am SLSP and solubility/speciation

As discussed above, the solubility of Am depends directly on the solid phase that is in contact with the aqueous solution. Dissolution can take a long time to reach true equilibrium, therefore, some metastable amorphous phases can persist for some prolonged times and serve as the SLSP. Thermodynamically, the most stable solid phase is expected to be the SLSP, as less stable phases would eventually be replaced by the most stable phase. However, in reality, this may not always be the case as kinetics can often play a more important role in determining the behavior of a system. For example, recent experiments under the proposed Belgian and Chinese DGR conditions (Salah and Wang, 2017; Zhou et al., 2015) have shown that some amorphous phases are the solubility controlling phases for Am. Like uranium solid phases (Opel et al., 2007), amorphous Am solids almost always exhibit elevated solubilities compared to their crystalline counterparts (Table 5). By sequentially suppressing the most stable solid in our modeling calculations, it is possible to compute the pseudo-solubilities and speciation of Am with the potentially important metastable solid phases. Under the Beishan near-field and far-field conditions, we have carried out such calculations, the results are tabulated in Table 5; through similar calculations the results for the Boom Clay porewater at the Belgium Mol site have also been obtained and included in Table 5 for comparison. It is worth noting that while Am_2O_3(cr) is stable under the calculation conditions used in this study, its solubility is too high to be accurately modeled by using PHREEQC-3. Even when the concentration of Am(III) in solution is raised to 1 mol/kg and all other less soluble solid phases are suppressed, Am_2O_3(cr) does not form.

Based on their kinetic solubility experimental results, Salah and Wang (2017) concluded that $AmCO_3OH$(*am, hyd*) would be the Am SLSP in the Boom Clay porewater at the Mol site, Belgium, with an Am solubility of 3.8×10^{-6} mol/kg. This value should be considered conservative, as the other solids such as $NaAm(CO_3)_2{\cdot}5H_2O(cr)$ are thermodynamically more stable, and may gradually become predominant over time which would result in reduced Am solubility in Boom Clay porewater. When $AmCO_3OH$(*am, hyd*) is assumed as the SLSP in the Boom Clay porewater, the main dissolved Am species were calculated as: $Am(CO_3)_2^-$, $AmCO_3^+$, $Am(CO_3)_3^{3-}$ and $AmSiO(OH)_3^{2+}$ (Table 6).

The solid phase that is likely to control americium solubility during the first 5000 years following the closure of the Beishan repository remains uncertain. However, based on similarities to the Boom Clay porewater (Salah and Wang, 2017), we assume that $AmCO_3OH$(am, hyd) would be the SLSP. This assumption is more realistic than using the equilibrium model with crystalline phases as SLSPs as presented earlier. Under this assumption, we calculated the solubility of Am to be 6.3×10^{-7} mol/kg and 2.4×10^{-6} mol/kg for the near- and far-field conditions, respectively, as presented in Table 6. Kim and Cho (2022) conducted an experiment using synthetic groundwater similar to that of Beishan with a pH of 9.03 and $[HCO_3^-]$ of 1.38×10^{-3} mol/L. They started the experiment from super-saturation and measured an Am solubility of approximately 2×10^{-7} mol/L after 70 days at 25 °C. Although they were unable to characterize the precipitate due to a limited quantity, their measured Am solubility is in excellent agreement with our

Table 5
Am solubilities with different solid phases under conditions of Beishan, China and Mol site, Belgium.

Beishan granitic groundwater, China				Boom Clay porewater at Mol site, Belgium[c]	
Near-field[a]		Far-field[b]			
SLSP	Sty/mol/kg[d]	SLSP	Sty/mol/kg[d]	SLSP	Sty/mol/kg[d]
$Am(OH)_3$ (am)	8.4×10^{-6}	$Am(OH)_3$ (am)	3.2×10^{-4}	$Am(OH)_3$ (am)	1.3×10^{-3}
$Am_2(CO_3)_3$ (am)	2.0×10^{-6}	$Am(OH)_3$ (cr)	1.8×10^{-5}	$Am(OH)_3$ (cr)	6.2×10^{-5}
$AmCO_3OH$(am,hyd)	6.3×10^{-7}	$AmCO_3OH$(am,hyd)	2.4×10^{-6}	$AmCO_3OH$(am,hyd)	3.8×10^{-6}
$NaAm(CO_3)_2{\cdot}5H_2O$(cr)	4.4×10^{-7}	$Am_2(CO_3)_3$ (am)	2.2×10^{-6}	$Am_2(CO_3)_3$ (am)	2.5×10^{-6}
$Am(OH)_3$ (cr)	4.2×10^{-7}	$NaAm(CO_3)_2{\cdot}5H_2O$(cr)	1.2×10^{-6}	$Am(CO_3)_{1.5}$ (cr)	2.4×10^{-6}
$AmCO_3OH{\cdot}0.5H_2O$(cr)	4.0×10^{-9}	$AmCO_3OH{\cdot}0.5H_2O$(cr)	1.5×10^{-8}	$NaAm(CO_3)_2{\cdot}5H_2O$(cr)	7.7×10^{-7}
Am_2O_3(cr)	Soluble	Am_2O_3(cr)	Soluble	$AmCO_3OH{\cdot}0.5H_2O$(cr)	2.4×10^{-8}

[a] pH = 8.9, Eh = −182 mV, $[HCO_3^-] = 2.31 \times 10^{-3}$ mol/kg.
[b] pH = 7.8, E_h = 98 mV, $[HCO_3^-] = 2.15 \times 10^{-3}$ mol/kg.
[c] pH = 8.36, E_h = −281 mV, $P_{CO2} = 10^{-2.62}$ bar, SiO_2(*aq*)-Cl-Na type porewater (Wang, 2022).
[d] Sty, Solubility.

Table 6
Calculated Am solubilities and main dissolved species in near- and far-field groundwaters, Beishan, China and Boom Clay porewater at the Mol site, Belgium, when $AmCO_3OH$(am, hyd) is assumed to be the SLSP.

Beishan granitic groundwater, China				Boom Clay porewater at the Mol site, Belgium[c]	
Near-field[a]		Far-field[b]			
SLSP	$AmCO_3OH$ (am, hyd)	SLSP	$AmCO_3OH$ (am, hyd)	SLSP	$AmCO_3OH$ (am, hyd)
Solubility	6.3×10^{-7} m	Solubility	2.4×10^{-6} m	Solubility	3.8×10^{-6} m
$Am(CO_3)_2^-$	78%	$AmCO_3^+$	52%	$Am(CO_3)_2^-$	84%
$AmCO_3^+$	15%	$AmSiO(OH)_3^{2+}$	24%	$AmCO_3^+$	12%
$AmSiO(OH)_3^{2+}$	4%	$Am(CO_3)_2^-$	20%	$Am(CO_3)_3^{3-}$	3%
				$AmSiO(OH)_3^{2+}$	0.4%

[a] pH = 8.9, Eh = −182 mV, $[HCO_3^-] = 2.31 \times 10^{-3}$ mol/kg.
[b] pH = 7.8, E_h = 98 mV, $[HCO_3^-] = 2.15 \times 10^{-3}$ mol/kg.
[c] pH = 8.36, E_h = −281 mV, $P_{CO2} = 10^{-2.62}$ bar, $SiO_2(aq)$-Cl-Na type porewater (Wang, 2022).

near-field results, assuming that $AmCO_3OH$(am, hyd) is the SLSP.

Table 6 also presents our calculated primary aqueous Am(III) species. Under the near-field conditions, the predominant species is $Am(CO_3)_2^-$, accounting for 78% of the total dissolved Am(III), while under the far-field conditions, $AmCO_3^+$ is the primary species, accounting for 52%. However, other more soluble solid phases such as $Am_2(CO_3)_3$ (*am*) and $Am(OH)_3$ (am) may become the SLSPs under certain thermodynamic and kinetic conditions, resulting in even higher Am solubility than shown in Table 6 (cf. Table 5). Conversely, the thermodynamically stable crystalline phase $AmCO_3OH{\cdot}0.5H_2O$(*cr*) may reach equilibrium with the environment over ~5000 years, leading to much lower Am solubility in the Beishan groundwater, particularly under the far-field conditions. These discussions are based on the pH values reported in Table 1. Fig. 5 shows how pH changes would impact the speciation of Am(III) for both near-field (Fig. 5b) and far-field (Fig. 5a) conditions in the proposed Beishan DGR.

In summary, we have examined the stable and metastable solid phases of Am, as well as their solubilities and pseudo-solubilities in aqueous solutions. The variation of these properties as a function of pH and P_{CO2} is presented in Fig. 6, which was constructed using PhreePlot and is pertinent to the Am(III) aqueous species present in Beishan groundwater.

It is important to acknowledge that our modeling calculations do not include certain complexing ligands and aqueous species, such as boron and the ternary Ca-Am-OH complexes, due to the limited availability of data. Therefore, the results presented in Fig. 6 may be subject to change as additional data become available.

Our computation results show that Am solubilities are of similar order of magnitude to that of uranium in groundwaters (Opel et al., 2007). However, because of its much higher radiotoxicity, before it can be safely ignored (after ~5000 yrs or 10 half-lives of Am-241), Am could pose a significant health hazard to the nearby communities if it enters the local drinking water system (WHO, 2022). In this regard, it is imperative that the engineered barriers must be able to contain the HLW within this timeframe. This point is particularly important considering that the more soluble amorphous Am solid phases may act as the SLSPs as discussed above. However, this caveat is based on the assumption that there would be unlimited Am available for dissolution and migration during this entire period of time. Since the minor components including the fission products and actinides in spent fuels are locked in the UO_2 matrix of SNF, the main component of HLW, they are released only when the bulk UO_2 dissolves (Goodwin, 1982). Similarly, the borosilicate glass of vitrified HLW is very stable over a very long period and is expected to be highly effective in containing the radionuclides in the waste (Alexander et al., 2015). Besides, it is also possible that the metastable amorphous Am solids would gradually convert to the less soluble crystalline forms that could reduce Am solubility significantly within several hundreds of years after a DGR's closure. Finally, it has been shown (e.g., Cigar Lake, Canada) that uraninite ores (i.e., UO_2) have undergone only minor dissolution and alteration over the course of one billion years since their formation, suggesting that uraninite ores has effectively contained all radionuclides, including minor components, within themselves (Alexander et al., 2015).

3.4. Colloidal formation and sorption of Am(III) on Am mobility

Like the other aqueous actinide ions, Am^{3+} is unstable in aqueous systems due to strong hydrolysis reactions, and the hydrolyzed products may polymerize to form radioactive colloids or be further adsorbed onto the other colloids ubiquitously present in natural aquifers to form radioactive pseudo-colloids (Kim, 1991). In addition, Am^{3+} also has a tendency to be adsorbed onto the surfaces of minerals in groundwaters (Kim, 1991). The formation of these radioactive colloids and pseudo-colloids may enhance the mobility of Am in Beishan groundwater (Guan et al., 2009, 2011), while the sorption of Am(III) to solids may suppress Am mobility and hence attenuate its migration in a natural aquifer. However, rigorous assessment of these effects is not an easy task. The formation of colloids and surface adsorption are governed by the intrinsic factors including the thermodynamics and kinetics of the

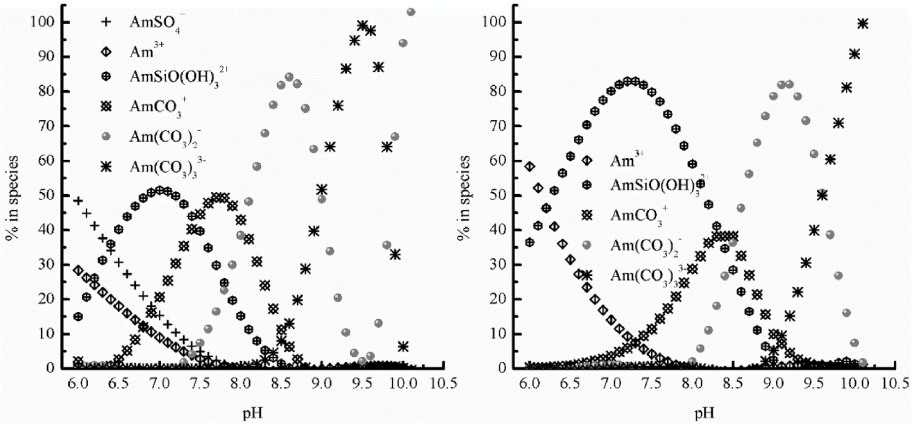


Fig. 5. Am(III) speciation vs. pH, chemical compositions from Table 1, (a) Beishan DGR far-field condition (total [Am(III)] = 1.0×10^{-9} mol/kg, E_h = 98 mV, T = 25 °C); (b) Beishan DGR near-field condition (total [Am(III)] = 1.0×10^{-9} mol/kg, E_h = −182 mV, T = 25 °C).

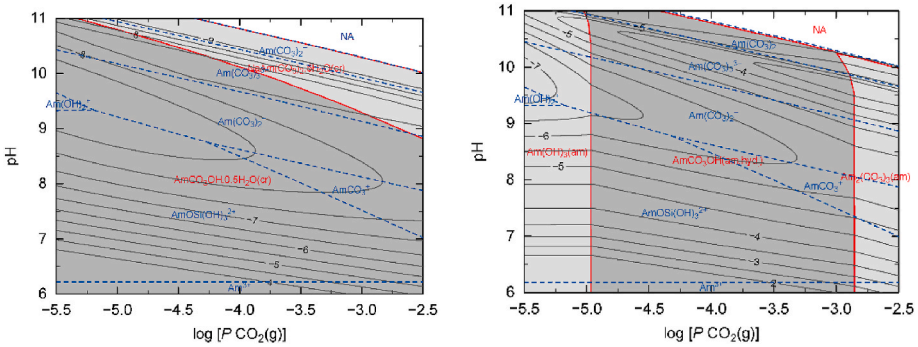


Fig. 6. PH-logP_{CO2} diagram (left, crystalline solid phases, right, amorphous solid phases) of Am(III) solids and aqueous species with Am solubility contour lines (grey, in log mol/kg) in Beishan synthetic water at 25 °C and 1 bar (0.01 mol/kg NaCl and 0.001 mol/kg Na_2SO_4 as background electrolytes), calculated using PhreePlot with the thermodynamic data in Table 2. Red lines separate solid phases, and the blue dashed lines separate the aqueous species.

colloidal formation of Am(III) as well as the external factors including pH, ionic strength, temperature and pressure, and the presence or absence of organic substances. Despite large amount of work in the literature on these subjects (e.g., Kim, 1991; Wang et al., 2010; Guan et al., 2009, 2011) there are still many questions remaining unanswered. Moreover, it is worth noting that without a reasonable understanding on Am(III) colloidal formation and sorption, the migration of Am due to dissolution of HLW in groundwaters cannot be fully assessed.

Due to its high radiotoxicity and hence difficulty in laboratory handling, Am is often studied using the analogues such as Eu, which is an excellent lanthanide analogue to the highly radiotoxic trivalent actinides (Bierkens and Simkiss, 1990). Liu et al. (2008) conducted several solubility experiments with $Eu(OH)_3(s)$ in the presence and absence of organic matter under the Boom Clay conditions (pH = ~8.3, logP_{CO2} = −4.52 atm), and suggested that the formation of small (30 kD - 0.45 μm) and very small (<30 kD) inorganic colloids in the form of $Eu(OH)_x(CO_3)_y$ caused the increase of dissolved Eu by an order of magnitude. Will the formation of Am(III) colloids increase Am mobility in groundwaters by a similar magnitude?

We have conducted calculations using PHREEQC-3 under the Beishan granitic groundwater and Boom Clay porewater conditions, assuming the presence of Am colloidal species similar to Eu(OH)x (CO3) y in the system. The formation constant for $AmOHCO_3$(coll.) was taken from LLNL-TDB (Wolery, 2020). Our calculation results show that $AmOHCO_3$(coll.) would be the dominant species in the aqueous phase, and $AmCO_3OH{\cdot}0.5H_2O$(cr) would be the solid phase in both the Beishan groundwater and the synthetic Boom Clay porewater. When accounting for the colloidal species, our calculated Am "colloidal solubility" was about 12 times greater than the solubility without including colloids (2.9×10^{-7} mol/kg vs. 2.4×10^{-8} mol/kg) in the Boom Clay porewater. This enhancement factor agrees well with the work of Liu et al. (2008), who observed a 10 to 15-fold increase in Eu mobility due to colloids in the Boom Clay porewater. Under the Beishan near-field granitic groundwater conditions, our calculations show that the enhancement factor for Am is ~68 (2.7×10^{-7} mol/kg vs. 4.0×10^{-9} mol/kg assuming true equilibrium condition), and ~19 under far-field conditions (2.8×10^{-7} mol/kg vs. 1.5×10^{-8} mol/kg). Notably, our calculated Am solubility of 1.7×10^{-8} mol/kg in the Boom Clay porewater agrees well with the experimental results of Maes et al. (2004), who determined Am solubility in synthetic Boom Clay porewater to be 2.0×10^{-8} mol/kg after ultrafiltration at 30 kD.

However, Kim (1991) found that although Am(III) had a strong tendency to form colloids in near neutral pH solutions, these colloids were much less stable compared to the tetravalent Th and Pu colloids, and prone to adsorption onto solid surfaces such as experimental vessel walls. These observations are in agreement with the work of Guan et al. (2011) where Am(III) was shown to form colloids with OH^-, and the formation of these Am(III)–OH^- colloids was shown to be more favored in basic solutions over the pH range of 6–9. The adsorption of Am onto the minerals through surface complexation can lead to a reduction in its mobility (Zachara et al., 2007). It seems that the formation of colloids and the sorption processes play two closely related yet opposite roles in mobilizing Am in natural systems, while the sorption processes of Am (III) might be more important with regard to its mobility and migration. This statement may be an over-simplification of natural processes, as both Kim (1991) and Runde (2000) indicated that Am(III) strong sorption only occurs near neutral pH in aqueous solutions. Both colloidal formation and sorption of Am(III) in groundwaters depend on so many convoluted factors including the presence or absence of dissolved humic substances and other strong complexing ligands, the permeabilities of the engineered barriers and rock formations, the sorption, diffusion and filtration capabilities of the natural aquifers, many of these have not been well understood (Kim, 1991; Runde, 2000; Siegel and Bryan, 2003).

4. Conclusions

We used the geochemical codes PHREEQC-3 and PhreePlot, along with rigorously assessed thermodynamic data (mostly from the OECD-TDB project), to calculate the solubility and speciation of americium under both near- and far-field conditions at the proposed China's DGR in Beishan, Gansu Province. We assumed that the thermodynamically metastable amorphous phase $AmCO_3OH$(*am, hyd*) is the solubility limiting solid under both conditions. Our calculations show that the solubility of Am under Beishan near- and far-field conditions is 6.3×10^{-7} mol/kg and 2.4×10^{-6} mol/kg, respectively. These results indicate that americium can pose a significant environmental hazard if not contained within ~5000 years after the closure of a DGR. Therefore, due to its high radiotoxicity, it is crucial to ensure that the engineered barriers of a DGR can effectively contain Am-241 in the HLW disposed of within this timeframe.

While the solubility of Am in Beishan DGR is relatively low under both near- and far-field conditions, sorption and colloidal formation may play a more significant role in mobilizing Am in natural aquifers. However, accurately assessing these effects requires a thorough understanding of several parameters, such as the concentration of dissolved humic substances and other strong complexing ligands in the groundwater. Unfortunately, these factors are not currently well-understood for Beishan, making further research necessary to gain a better understanding of these effects.

Declaration of competing interest

The authors declare that they have no known competing financial interests or personal relationships that could have appeared to influence the work reported in this paper.

Data availability

Data will be made available on request.

Acknowledgements

We wish to express our sincere gratitude to Drs. Law, Wang, and Zavarin for their effort in handling and reviewing this submission. Their invaluable contributions have significantly improved the quality of this manuscript. We also extend our appreciation to the two anonymous reviewers whose insightful comments and suggestions have been instrumental in enhancing the manuscript. In the latter part of this work, the first author received invaluable assistance from Dr. David Kinniburgh, and we are deeply grateful for his guidance and assistance.

References

Alexander, W.R., Reijonen, H.M., McKinley, I.G., 2015. Natural analogues: studies of geological processes relevant to radioactive waste disposal in deep geological repositories. Swiss J. Geosci. 108, 75–100. https://doi.org/10.1007/s00015-015-0187-y.

Altmaier, M., Vercouter, T., 2012. Aquatic chemistry of the actinides: aspects relevant to their environmental behaviour. In: Poinssot, C., Geckeis, H. (Eds.), Radionuclide Behaviour in the Natural Environment: Science, Implications and Lessons for the Nuclear Industry. Woodhead Publishing, Cambridge. https://doi.org/10.1533/9780857097194.1.44.

Altmaier, M., Gaona, X., Fanghänel, T., 2013. Recent advances in aqueous actinide chemistry and thermodynamics. Chem. Rev. 113, 901–943.

Andersson, J., Ström, A., Svemar, C., Almen, K.E., Ericsson, L.O., 2000. What Requirements Does the KBS-3 Repository Make on the Host Rock? Geoscientific Suitability Indicators and Criteria for Siting and Site Evaluation (No. SKB-TR-00-12). Swedish Nuclear Fuel and Waste Management Co. https://inis.iaea.org/collection/NCLCollectionStore/_Public/32/003/32003266.pdf?r=1.

Berner, U., 2014. Solubility of Radionuclides in a Concrete Environment for Provisional Safety Analyses for SGT-E2 (No. NTB–14-07). Paul Scherrer Institute (PSI), pp. 4–8.

Bierkens, J., Simkiss, K., 1990. The use of chemical analogues such as Eu/Am in ecotoxicological studies. Funct. Ecol. 4 (3), 445–447. https://doi.org/10.2307/2389607.

Birkholzer, J., Houseworth, J., Tsang, C.F., 2012. Geologic disposal of high-level radioactive waste: status, key issues, and trends. ANNU REV ENV RESOUR 37, 79–80. https://doi.org/10.1146/annurev-environ-090611-143314.

Borkowski, M., Richmann, M., Reed, D.T., Xiong, Y., 2010. Complexation of Nd(III) with tetraborate ion and its effect on actinide(III) solubility in WIPP brine. Radiochim. Acta 98, 577–582.

Bruggeman, C., Salah, S., Maes, N., 2012. Americium retention and migration behaviour in Boom Clay. External report of the Belgian nuclear research centre, SCK· CENER-201. Mol, Belgium 16–22.

Cantrell, K.J., Felmy, A.R., 2012. Plutonium and Americium Geochemistry at Hanford: A Site Wide Review. United States. https://www.osti.gov/servlets/purl/1051201.

Duan, X.Z., Niu, S.J., Wang, C.Z., Wang, J., Zhou, Z.C., ling, H., 2021. Safety evaluation study on the geological disposal of high-level radioactive waste: a case study of Beishan, Gansu province. China Mining Magazine 30 (4), 8–9. https://doi.org/10.12075/j.issn.1004-4051.2021.04.026 (in Chinese).

Emerson, H.P., Sinkov, S.I., Pearce, C.I., Cantrell, K.J., Delegard, C.H., Snyder, M.M.V., Thomas, M.-L., Reilly, D.D., Buck, E., LucasSweet, L., Amanda, J., Casella, A.J., Carter, J.C., Corbey, J.F., Schwerdt, I.J., Clark, R., Heller, F.D., Meier, D., Zavarin, M., Kersting, A.B., Freedman, V.L., 2022. Solubility controls on plutonium and americium release in subsurface environments exposed to acidic processing wastes. Appl. Geochem. 2022 (47), 105241 https://doi.org/10.1016/j.apgeochem.2022.105241.

Giffaut, E., 1994. Influence des ions chlorure sur la chimie des actinides: Effets de la radiolyse et de la température. Ph.D thesis (Universite de Paris-Sud).

Goodwin, B., 1982. Calculated uranium solubility in groundwater: implications for nuclear fuel waste disposal. Can. J. Chem. 60, 1759.

Grenthe, I., Gaona, X., Plyasunov, A.V., Rao, L., Runde, W.H., Grambow, B., Konings, R.J. M., Smith, A.L., Moore, E.E., 2020. Second Update on the Chemical Thermodynamics of U, Np, Pu, Am and Tc. A new NEA publication: Chemical Thermodynamics, pp. 131–134.

Guan, H.Z., Zhang, Z.T., Su, X.G., Long, H.Q., Wang, B., Yao, J., Song, Z.X., Chen, X., 2009. Sorption behavior of americium on granite. J. Nucl. Radiochem. 31 (3), 189–192.

Guan, H.Z., Zhou, D., Long, H.Q., Yao, J., Wang, B., Jiang, T., Song, Z.X., 2011. Colloidal behavior of americium. J. Nucl. Radiochem. 33 (2), 84–88.

Guillaumont, R., Mompean, F.J., 2003. Update on the Chemical Thermodynamics of Uranium, Neptunium, Plutonium, Americium and Technetium, vol. 5. Elsevier, Amsterdam, p. 369.

Guo, Y.H., Su, R., Ji, R.L., Wang, H.L., Liu, S.F., Zong, Z.H., Dong, J.N., Zhang, M., 2014. Synthetic hydrogeological study on Beishan preselected area for high-level radioactive waste repository in China. World Nuclear Geoscience 31 (4), 587–593. https://doi.org/10.3969/j.issn.1672-0636.2014.04.005.

Hinz, K., Altmaier, M., Gaona, X., Rabung, T., Schild, D., Richmann, M., Reed, D.T., Alekseev, E.V., Geckeis, H., 2015. Interaction of Nd(III) and Cm(III) with borate in dilute to concentrated alkaline NaCl, $MgCl_2$and $CaCl_2$ solutions: solubility and TRLFS studies. New J. Chem. 39, 849–859. https://doi.org/10.1039/c4nj01203h.

Jiang, M.L., Wang, X.Y., Liu, C.L., Wang, D.W., Liu, F.Q., Zhang, H., 2014. Prediction of the species and solubility of Am in two different groundwaters. J. Nucl. Radiochem. 36 (5), 263–271. CNKI:SUN:HXFS.0.2014-05-002.

Kim, J.I., 1991. Actinide colloid generation in groundwater. Radiochim. Acta 52 (1), 71–82. https://doi.org/10.1524/ract.1991.5253.1.71.

Kim, H.-K., Cho, H.-R., 2022. Evaluation of americium solubility in synthesized groundwater: geochemical modeling and experimental study at over-saturation conditions. JNFCWT 20 (4), 399–410. http://orcid.org/0000-0001-5840-7194.

Kinniburgh, D.G., Cooper, D.M., 2011. PhreePlot – creating graphical output with PHREEQC. http://www.phreeplot.org/ original date June 2011, last updated December 17, 2014, 606 pp.

Liu, Y.M., Wang, J., Tan, G.H., Cai, M.F., 2007. Basic physico-mechanical properties and time-temperature effect of deep intact rock from Beishan preselected area for high-level radioactive waste disposal. Chin. J. Rock Mech. Eng. 26 (10), 2034–2042 (in Chinese).

Liu, D.J., Bruggeman, C., Maes, N., 2008. The influence of natural organic matter on the speciation and solubility of Eu in Boom Clay porewater. Radiochim. Acta 96 (9–11), 711–720. https://doi.org/10.1524/ract.2008.1557.

Lu, Y., Dong, J., Ke, W., 2015. Corrosion evolution of low alloy steel in deaerated bicarbonate solutions. J. Mater. Sci. Technol. 31 (10), 1047–1058. https://doi.org/10.1016/j.jmst.2014.10.013.

Maes, N., Wang, L., Delécaut, G., Beauwens, T., Van Geet, M., Put, M., Weetjens, E., Marivoet, J., van der Lee, J., Warwick, P., Hall, A., Walker, G., Maes, A., Bruggeman, C., Bennett, D., Hicks, T., Higgo, J., Galson, D., 2004. Migration Case Study: Transport of Radionuclides in a Reducing Clay Sediment (TRANCOM-II) - Final Scientific and Technical Report of the EC TRANCOM-II Project. Office for Official Publications of the European Communities, BLG-988, SCK-CEN, Mol, Belgium.

Maher, Z., Ivanov, P., O'Brien, L., Sims, H., Taylor, R.J., Heath, S.L., Bryan, N.D., 2016. Americium and plutonium association with magnesium hydroxide colloids in alkaline nuclear industry process environments. J. Nucl. Mater. 468, 84–96. https://doi.org/10.1016/j.jnucmat.2015.11.010.

Maloubier, M., Michel, H., Solari, P.L., Moisy, P., Tribalat, M.A., Oberhaensli, F.R., Dechraoui Bottein, M.Y., Thomas, O.P., Monfort, M., Moulin, C., Den Auwer, C., 2015. Speciation of americium in seawater and accumulation in the marine sponge Aplysina cavernicola. Dalton T 44 (47), 84–96. https://doi.org/10.1039/C5DT02805A.

McCartin, T., 2020. Management and Disposal of High-Level Radioactive Waste: Global Progress and Solutions. Nuclear Energy Agency and European Commission, OECD NEA No. 7532.

Meinrath, G., Kim, J.I., 1991. Solubility products of different Am(III) and Nd(III) carbonates. Eur. J. Solid State Inorg. Chem. 28, 383–388.

Merli, L., Fuger, J., 1996. Thermochemistry of selected lanthanide and actinide hydroxycarbonates and carbonates. Radiochim. Acta 74 (s1), 37–44. https://doi.org/10.1524/ract.1996.74.special-issue.37.

Neck, V., Altmaier, M., Rabung, T., Lützenkirchen, J., Fanghänel, T., 2009. Thermodynamics of trivalent actinides and neodymium in NaCl, $MgCl_2$, and $CaCl_2$ solutions: solubility, hydrolysis, and ternary Ca-M(III)-OH complexes. Pure Appl. Chem. 81 (9), 1555–1568. https://doi.org/10.1351/PAC-CON-08-09-05.

Novikov, A.P., Kalmykov, S.N., Kuzovkina, E.V., Myasoedov, B.F., Fujiwara, K., Fujiwara, A., 2009. Evolution of actinide partitioning with colloidal matter collected at PA "Mayak" site as studied by sequential extraction. J. Radioanal. Nucl. Chem. 280 (3), 629–634. https://doi.org/10.1007/s10967-008-7397-y.

Opel, K., Weiß, S., Hübener, S., Zänker, H., Bernhard, G., 2007. Study of the solubility of amorphous and crystalline uranium dioxide by combined spectroscopic methods. Radiochim. Acta 95 (3), 43–149. https://doi.org/10.1524/ract.2007.95.3.143.

Östhols, E., Wanner, H., 2000. TDB-0: the NEA thermochemical data Base project, nuclear Energy agency data bank, organisation for economic Co-operation and development. Tech. Rep. https://www.oecd-nea.org/jcms/pl_37490/tdb-0-the-nea-thermochemical-database-tdb-project?details=true.

Parkhurst, D.L., Appelo, C.A.J., 2013. Description of Input and Examples for PHREEQC Version 3: a Computer Program for Speciation, Batch-Reaction, One-Dimensional Transport, and Inverse Geochemical Calculations (No. 6-A43). US Geological Survey. https://doi.org/10.3133/tm6A43.

Pusch, R., Yong, R.N., Nakano, M., 2018. Geologic Disposal of High-Level Radioactive Waste. CRC Press, pp. 44–46. https://doi.org/10.1201/9781351256803.

Rabung, T., Altmaier, M., Neck, V., Fanghänel, T., 2008. A TRLFS study of Cm (III) hydroxide complexes in alkaline $CaCl_2$ solutions. Radiochim. Acta 96 (9–11), 551–560. https://doi.org/10.1524/ract.2008.1536.

Runde, W., 2000. The chemical interactions of actinides in the environment. Los Alamos Sci. 26, 392–411.

Salah, S., Wang, L., 2017. Speciation and Solubility Calculations for Waste Relevant Radionuclides in Boom Clay. SCK-CEN 26188888 Report ER, pp. 37–40.

Schott, J., Kretzschmar, J., Acker, M., Eidner, S., Kumke, M.U., Drobot, B., Barkleit, A., Taut, S., Brendler, V., Stumpf, T., 2014. Formation of a Eu(III) borate solid species from a weak Eu(III) borate complex in aqueous solution. Dalton Trans. 43, 11516–11528. https://doi.org/10.1039/c4dt00843j.

Schramke, J.A., Santillan, E.F.U., Peake, R.T., 2020. Plutonium oxidation states in the waste isolation pilot plant repository. Appl. Geochem. 116, 104561 https://doi.org/10.1016/j.apgeochem.2020.104561.

Siegel, M.D., Bryan, C.R., 2003. Environmental geochemistry of radioactive contamination. Treatise Geochem 9, 205–262.

Silva, R.J., Bidoglio, G., Robouch, P.B., Puigdomenech, I., Wanner, H., Rand, M.H., 2012. Chemical Thermodynamics of Americium. Newnes, pp. 147–166.

Thoenen, T., Hummel, W., Berner, U., Curti, E., 2014. The PSI/Nagra Chemical Thermodynamic Database 12/07. PSI Internal Report, TM-44-12-03. Paul Scherrer Institut, Villigen, Switzerland, pp. 86–104.

Tian, X., Wang, J., Jin, Y.X., Li, J.B., 2014. The isotopic geochemistry of filling calcite in Jiujing and Xinchang granite in Beishan site for high-level radioactive waste disposal. Uranium Geol. 30 (1), 23–29. https://doi.org/10.3969/j.isn.1000-0658.2014.01.004.

Trofimov, T.I., Kulyako, Y.M., Perevalov, S.A., Malikov, D.A., Myasoedov, B.F., 2008. Solubility of uranium, neptunium, and plutonium dioxides in simulated groundwater under various conditions. Radiochemistry 50 (2), 147–151. https://doi.org/10.1134/S1066362208020094.

Vercouter, T., Amekraz, B., Moulin, C., Vitorge, P., 2004. Lanthanide and Actinide Inorganic Complexes in Natural Waters. TRLFS and ESI-MS Studies (No. INIS-FR–3002). ANDRA.

Vercouter, T., Amekraz, B., Moulin, C., Giffaut, E., Vitorge, P., 2005a. Sulfate complexation of trivalent lanthanides probed by nanoelectrospray mass spectrometry and time-resolved laser-induced luminescence. Inorg. Chem. 44 (21), 7570–7581. https://doi.org/10.1021/ic048503j.

Vercouter, T., Vitorge, P., Trigoulet, N., Giffaut, E., Moulin, C., 2005b. $Eu(CO_3)_3^{3-}$ and the limiting carbonate complexes of other M^{3+} f-elements in aqueous solutions: a solubility and TRLFS study. New J. Chem. 29 (4), 544–553. https://doi.org/10.1039/b413002b.

Wang, J., 2010. High-level radioactive waste disposal in China: update 2010. JRMGE 2 (1), 1–11. https://doi.org/10.3724/SP.J.1235.2010.00001.

Wang, L., 2022. Speciation and Solubility Calculations for Waste Relevant Radionuclides in Boom Clay. SCK- CEN/45742196, pp. 10–12. https://publications.sckcen.be/portal/files/7352726/ResearchOutput-45742196.pdf.

Wang, B., Liu, D.J., Yao, J., Wei, F., Jiang, T., He, X.H., Chen, X., Guan, H.Z., Song, Z.X., Bao, L.J., Zhang, Y., Zhou, D.H., Long, H.Q., Fan, X.H., 2010. Colloidal behavior of neptunium in present of humic acids. Atomic Energy Sci. Technol. 44 (9), 1031–1038.

Wang, P., Anderko, A., Kosinski, J.J., Springer, R.D., Lencka, M.M., 2017. Modeling speciation and solubility in aqueous systems containing U(IV, VI), Np(IV, V, VI), Pu (III, IV, V, VI), Am(III), and Cm(III). J. Solut. Chem. 46, 521–588. https://doi.org/10.1007/s10953-017-0587-x.

Wang, J., Chen, L., Su, R., Zhao, X., 2018. The Beishan underground research laboratory for geological disposal of high-level radioactive waste in China: planning, site selection, site characterization and in situ tests. JRMGE 10 (3), 411–435. https://doi.org/10.1016/j.jrmge.2018.03.002.

Wanner, H., 2007. Solubility data in radioactive waste disposal. Pure Appl. Chem. 79 (5), 875–882. https://doi.org/10.1351/pac200779050875.

Wei, X., Liu, Y.M., Dong, J.H., Cao, S.F., Xie, J.L., Chen, N., Xue, F., Ke, W., 2019. Study on corrosion behavior of low carbon steel under different water conditions in bentonite of China-Mock-Up. Appl. Clay Sci. 167, 23–32. https://doi.org/10.1016/j.clay.2018.10.004.

WHO (World Health Organization), 2022. Guidelines for Drinking-Water Quality: Fourth Edition Incorporating the First and Second Addenda. CC BY-NC-SA 3.0 IGO, Licence, 978-92-4-004506-4.

Winberg, M.R., Garcia, R.S., 1995. National Low-Level Waste Management Program Radionuclide Report Series, vol. 14. Americium-241 (No. DOE/LLW–130). EG and G Idaho. https://inis.iaea.org/collection/NCLCollectionStore/_Public/27/032/27032341.pdf?r=1.

Wolery, T., 2020. M4SF-20LL010301042: Updated Thermodynamic Database for Use in Generic Disposal System Assessment (No. LLNL-TR-812024). Lawrence Livermore National Lab. (LLNL), Livermore, CA (United States), pp. 4–21.

Xiong, Y., Kirkes, L., Marrs, C., Knox, J., 2017. Am(III)/Nd(III) interactions with borate: experimental investigations of $Nd(OH)_3$(micro cr) solubility in NaCl solutions in equilibrium with borax. In: 6th East Asia Forum on Radwaste Management November 27-29, 2017, Osaka, Japan.

Yang, G., Kang, M.L., Cheng, X., Ma, Y., Liu, Y., Li, J.B., Wang, J., 2019. A novel methodology for investigating the redox potential of underground water in China's Beishan HLW repository site. J. Radioanal. Nucl. Chem. 322 (2), 923–932. https://doi.org/10.1007/s10967-019-06728-x.

Zachara, J.M., Serne, J., Freshley, M., Mann, F., Anderson, F., Wood, M., Jones, T., Myers, D., 2007. Geochemical Processes Controlling Migration of Tank Wastes in Hanford's Vadose Zone, vol. 301. US Department of Energy Publications. https://digitalcommons.unl.edu/usdoepub/301.

Zhou, D., Long, H.Q., Chen, X., Wang, B., Bao, L.J., Song, Z.X., 2015. Solubility of Am(III) in groundwater. Atomic Energy Sci. Technol. 49 (5), 775–779. https://doi.org/10.7538/yzk.2015.49.05.0775.